Inorganic Chemistry
Article

Inorg. Chem. **2010**, *49*, 8591–8600 **8591**
DOI: 10.1021/ic101253g

Asymmetrical $[Ni(dmit)_2]^-$ Arrangements Induced by (1*R*,2*R*)-Cyclohexanediammonium - Crown Ether Supramolecules

Qiong Ye,*,†,‖ Tomoyuki Akutagawa,*,‡ Toru Endo,# Shin-ichiro Noro,†,# Takayoshi Nakamura,*,†,# and Ren-Gen Xiong‖

†*Research Institute for Electronic Science, Hokkaido University, Sapporo 001-0020, Japan,* ‡*Institute of Multidisciplinary Research for Advanced Materials (IMRAS), Tohoku University, 2-1-1 Katahira, Aoba-ku, Sendai 980-8577, Japan,* #*Graduate Schools of Environmental Science, Hokkaido University, Sapporo 060-0810, Japan, and* ‖*Ordered Matter Science Research Center, Southeast University, Nanjing 210096, P. R. China*

Received June 24, 2010

Structurally flexible (1*R*,2*R*)-cyclohexanediammonium ($CHDA^{2+}$) dication formed hydrogen-bonding supramolecules with [18]crown-6, benzo[18]crown-6 (B[18]crown-6), dibenzo[18]crown-6 (DB[18]crown-6), and dicyclohexano-[18]crown-6 (DCH[18]crown-6) in $[Ni(dmit)_2]^-$ salts ($dmit^{2-}$=2-thioxo-1,3-dithiole-4,5-dithiolate). The two ammonium moieties of $CHDA^{2+}$ interacted with the crown ethers to form open-mouth-shaped sandwich-type cationic structures of $(CHDA^{2+})(\text{crown ethers})_2$, that is, $(CHDA^{2+})([18]\text{crown-6})_2[Ni(dmit)_2]_2^-$ (**1**), $(CHDA^{2+})(B[18]\text{crown-6})_2[Ni(dmit)_2]_2^-$ (**2**), $(CHDA^{2+})(DB[18]\text{crown-6})_2[Ni(dmit)_2]_2^-$ (**3**), and $(CHDA^{2+})(DCH[18]\text{crown-6})_2[Ni(dmit)_2]_2^-$ (**4**). The chiral structure of $CHDA^{2+}$ induced asymmetrical $[Ni(dmit)_2]^-$ arrangements in the crystals. A large frequency and temperature dependence of the dielectric response was observed in $(CHDA^{2+})(B[18]\text{crown-6})_2$, due to the pendulum motion of the cyclohexane ring along the nitrogen−nitrogen direction of $CHDA^{2+}$. Since the inversion center of the $[Ni(dmit)_2]^-$ arrangements was lost in the unit cell due to the chiral space group, the salts **1**−**4** showed rather complicated magnetic behaviors. The temperature-dependent magnetic properties of salts **3** and **4** were explained by the sum of the Curie−Weiss and singlet−triplet thermal excitation models, with positive (ferromagnetic) and negative (antiferromagnetic) magnetic exchange energies, respectively.

Introduction

Redox active π-planar metal-coordination compounds such as $[Ni(dmit)_2]$ and $[Ni(mnt)_2]$ are useful building blocks for the construction of electrical conducting and magnetic molecular solids ($dmit^{2-}$ = 2-thioxo-1,3-dithiole-4,5-dithiolate and mnt^{2-} = maleonitriledithiolate).[1−3] The $[Ni(dmit)_2]$ has stable oxidation states ranging from dianion and anion radical, to neutral in the solid state. The electrically conducting solids were obtained using a partially oxidized $[Ni(dmit)_2]^{-\delta}$ ($0 < \delta < 1$) species, whereas monovalent $[Ni(dmit)_2]^-$ anion radical bearing one $S = 1/2$ spin gave magnetic materials in the form of ionic crystals.[1] The highly polarized sulfur atoms of $[Ni(dmit)_2]^-$ interacted with the nearest-neighboring molecules to achieve a variety of intermolecular interactions in the solid state. Typical intermolecular interactions between the $[Ni(dmit)_2]^-$ anions observed so far are π-stacking, lateral sulfur−sulfur contacts along the short and/or long-axis of the

*To whom correspondence should be addressed. Phone: +81-22-217-5653. Fax: +81-22-217-5655. E-mail: ries_yeqiong@es.hokudai.ac.jp (Q.Y.); akuta@tagen.tohoku.ac.jp (T.A.); tnaka@es.hokudai.ac.jp (T.N.).

(1) (a) Coomber, A. T.; Beljonne, D.; Friend, R. H.; Brédas, J. L.; Charlton, A.; Robertson, N.; Underhill, A. E.; Kurmoo, M.; Day, P. *Nature* **1996**, *380*, 144. (b) Rosa, A.; Ricciardi, G.; Baerends, E. J. *Inorg. Chem.* **1998**, *37*, 1368. (c) Smucker, B. W.; Hudson, J. M.; Omary, M. A.; Dunbar, K. R. *Inorg. Chem.* **2003**, *42*, 4714. (d) Sarangi, R.; DeBeer, G. S.; Rudd, D.; Szilagyi, R. K.; Ribas, X.; Rovira, C.; Almeida, M.; Hodgson, K. O.; Hedman, B.; Solomon, E. I. *J. Am. Chem. Soc.* **2007**, *129*, 2316.

(2) (a) Cassoux, P.; Valade, L.; Kobayashi, H.; Kobayashi, A.; Clark, R. A.; Underhill, A. E. *Coord. Chem. Rev.* **1991**, *110*, 115. (b) Pullen, A. E.; Olk, R.-K. *Coord. Chem. Rev.* **1999**, *188*, 211. (c) Kobayashi, A.; Sato, A.; Kobayashi, H. *J. Solid State Chem.* **1999**, *145*, 564. (d) Faulmann, C.; Cassoux, P. *Prog. Inorg. Chem.* **2004**, *52*, 399. (e) Kato, R. *Chem. Rev.* **2004**, *104*, 5319. (f) Broderick, W. E.; Thompson, J. A.; Godfrey, M. R.; Sabat, M.; Hoffman, B. M. *J. Am. Chem. Soc.* **1989**, *111*, 7657.

(3) (a) Brossard, L.; Ribault, M.; Bousseau, M.; Valade, L.; Cassoux, P. *C. R. Acad. Sci. Ser. B* **1986**, *302*, 205. (b) Brossard, L.; Ribault, M.; Valade, L.; Cassoux, P. *Phys. Rev. B* **1990**, *42*, 3935. (c) Kobayashi, A.; Kim, H.; Sasaki, Y.; Kato, R.; Kobayashi, H.; Moriyama, S.; Nishio, Y.; Kajita, K.; Sasaki, W. *Chem. Lett.* **1987**, *16*, 1819. (d) Kobayashi, A; Kato, R.; Miyamoto, A.; Kobayashi, A.; Kato, R.; Miyamoto, A.; Naito, T.; Kobayashi, H.; Clark, R. A.; Underhill, A. E. *Chem. Lett.* **1991**, 2163. (e) Kobayashi, H.; Bun, K.; Naito, T.; Kato, R.; Kobayashi, A. *Chem. Lett.* **1992**, 1909. (f) Tajima, H.; Inokuchi, M.; Kobayashi, A.; Ohta, T.; Kato, R.; Kobayashi, H.; Kuroda, H. *Chem. Lett.* **1993**, 1235. (g) Kato, R.; Kashimura, Y.; Aonuma, S.; Tajima, H.; Hanasaki, N. *Solid State Commun.* **1998**, *105*, 561. (h) Takahashi, K.; Cui, H.-B.; Okano, Y.; Kobayashi, H.; Mori, H.; Tajima, H.i; Einaga, Y.; Sato, O. *J. Am. Chem. Soc.* **2008**, *130*, 6688. (i) Kosaka, Y.; Yamamoto, H.; Nakao, A.; Tamura, M.; Kato, R. *J. Am. Chem. Soc.* **2007**, *129*, 3054.

Published on Web 08/19/2010

anion, and orthogonal π-overlap.[2,3] The $[Ni(dmit)_2]^-$ arrangements in the crystals, which determine the magnetic properties, were strongly affected by the structure of the counter cations. We have been utilizing the supramolecular cation approach for constructing $[Ni(dmit)_2]$ arrangements.[4−7] The supramolecular cations were designed based on crown ethers, which successfully introduced $[Ni(dmit)_2]^-$ crystals to a wide range of assembly structures with different strengths and directionalities of the intermolecular interactions.

Crown ethers can include inorganic ions such as Li^+, Na^+, K^+, Rb^+, Cs^+, Ca^{2+}, Co^{2+}, and Gd^{3+} through the ion−oxygen electrostatic interactions at their cavity, and these ions were introduced in $[Ni(dmit)_2]$ salts.[6] The crystal structures largely depended on the included metal cations and showed drastic changes in $[Ni(dmit)_2]^-$ arrangements. The ammonium moieties of organic ammonium ions ($R\text{-}NH_3^+$) were included in the crown ether cavity through $N-H^+$ - O hydrogen-bonding interactions to form supramolecular cation structures.[7,8] From a structural design viewpoint, the $R\text{-}NH_3^+$ - crown ether cationic structures exhibited diversity in terms of size, flexibility, chirality, and motional freedom in the solid state. These supramolecular cations formed $[Ni(dmit)_2]^-$ arrangements with a variety of magnetic interactions ranging from monomer, dimer, one-dimensional antiferromagnetic Heisenberg chains, two-leg spin-ladder, two-dimensional antiferromagnetic Heisenberg lattice, and ferromagnetic coupling.[6,7] For instance, the (anilinium$^+$)-([18]crown-6) supramolecule yielded a two-leg spin-ladder arrangement,[7a] whereas the (anilinium$^+$)(dicyclohexano[18]-crown-6) formed a lateral $[Ni(dmit)_2]^-$ anion arrangement with ferromagnetic coupling.[8b] The introduction of chiral $R\text{-}NH_3^+$ cations may achieve chiral and/or complicated $[Ni(dmit)_2]^-$ arrangements in the crystals. We previously examined (1*S*,2*S*)-diphenyl-1,2-ethanediammonium in $[Ni(dmit)_2]^-$ salts, which formed a two-dimensional antiferromagnetic Heisenberg lattice.[7d] The chiral ammonium cations in the $R\text{-}NH_3^+$ - crown ether assemblies have the potential to realize novel $[Ni(dmit)_2]^-$ arrangements in the solid state.

Another notable feature of the $R\text{-}NH_3^+$ - crown ether supramolecules is their motional freedom in the solid state. Solid state molecular rotators have been reported in molecular gyroscope compounds.[9] We already reported the molecular rotator structures of (anilinium)([18]crown-6), (*m*-fluoroanilinium)(dibenzo[18]crown-6), and (adamantylammonium)-([18]crown-6), in $[Ni(dmit)_2]^-$ crystals.[7,8] In the (*m*-fluoroanilinium)(dibenzo[18]crown-6)$[Ni(dmit)_2]^-$ crystal,[8a] the 2-fold flip-flop motion of *m*-fluoroanilinium was accompanied by dipole inversion, which was responsible for the dielectric response.[8c] The slow molecular rotation of *m*-fluoroanilinium caused a large dielectric response at lower frequencies and the crystal showed a ferroelectric−paraelectric phase transition at 346 K.[8c] The adamantylammonium moiety realized a 3- or 6-fold rotation in $[Ni(dmit)_2]^-$ salts due to its spherical shape.[8b] The flexibility of molecules is another notable feature for structural design of $R\text{-}NH_3^+$ based supramolecular cations. The conformational change in cyclohexanediamine should be an ideal candidate for this.[10] Herein, we focused on the optical active (1*R*,2*R*)-cyclohexanediammonium ($CHDA^{2+}$) dication in $[Ni(dmit)_2]^-$ salts.

Scheme 1. Conformational Change of (1*R*,2*R*)-Cyclohexanediamine from the (*e*,*e*)- to (*a*,*a*)-Conformation[a]

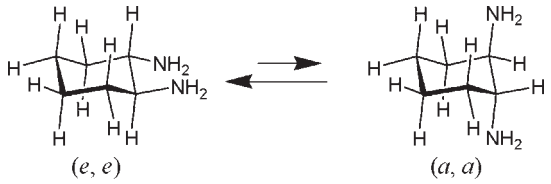

[a] The energy difference between the two conformations is about 22 kJ mol^{-1} from DFT calculations based on B3LYP basis sets.

Two chair conformations of (1*R*,2*R*)-cyclohexanediamine are possible, with (*a*,*a*)- and (*e*,*e*)-conformations of the two amino groups, where *a* indicates axial and *e* is for equatorial. The (*e*,*e*)-conformation is about 22 kJ mol^{-1} more stable than the (*a*,*a*)-one (Scheme 1), which is comparable to the rotational barrier of the phenyl ring (40 kJ mol^{-1}) in (anilinium)([18]crown-6)$[Ni(dmit)_2]^-$ salt.[7e] Therefore, this dynamic property concerning the conformational flexibility of $CHDA^{2+}$ was also expected to occur in $[Ni(dmit)_2]^-$ salts. We combined the $CHDA^{2+}$ dication with [18]crown-6, benzo[18]crown-6 (B[18]crown-6), dibenzo[18]crown-6 (DB-[18]crown-6), and *meso-cis*-cyclohexano[18]crown-6 (DCH[18]-crown-6) to form supramolecular cationic structures in $[Ni(dmit)_2]^-$ salts (Scheme 2). The cation conformation, $[Ni(dmit)_2]^-$ arrangements, dielectric and magnetic properties of the four new salts of $(CHDA^{2+})([18]crown\text{-}6)_2[Ni(dmit)_2]_2^-(CH_3CN)_{0.5}$ (**1**), $(CHDA^{2+})(B[18]crown\text{-}6)_2[Ni(dmit)_2]_2^-(CH_3CN)$ (**2**), $(CHDA^{2+})(DB[18]crown\text{-}6)_2[Ni(dmit)_2]_2^-$ (**3**), and $(CHDA^{2+})(DCH[18]crown\text{-}6)_2[Ni(dmit)_2]_2^-$ (**4**) were examined.

Experimental Section

Preparation of $(CHDA^{2+})(BF_4^-)_2$. Optical pure (1*R*,2*R*)-cyclohexanediamine (SIGMA-Aldrich, $[\alpha]^{20}_D$ −25°) was used for the preparation of diammonium salt. A 42% aqueous solution of

(4) Akutagawa, T.; Hasegawa, T.; Nakamura, T.; Inabe, T. *J. Am. Chem. Soc.* **2002**, *124*, 8903.
(5) Akutagawa, T.; Nakamura, T. *Dalton Trans.* **2008**, 6335.
(6) (a) Takamatsu, N.; Akutagawa, T.; Hasegawa, T.; Nakamura, T.; Inabe, T.; Fujita, W.; Awaga, K. *Inorg. Chem.* **2000**, *39*, 870. (b) Akutagawa, T.; Nishihara, S.; Takamatsu, N.; Hasegawa, T.; Nakamura, T.; Inabe, T. *J. Phys. Chem. B* **2000**, *104*, 5871. (c) Akutagawa, T.; Takamatsu, N.; Shitagami, K.; Hasegawa, T.; Nakamura, T.; Inabe, T. *J. Mater. Chem.* **2001**, *11*, 2118. (d) Nishihara, T.; Akutagawa, T.; Hasegawa, T.; Nakamura, T. *Inorg. Chem.* **2003**, *42*, 2480. (e) Akutagawa, T.; Shitagami, K.; Nishihara, S.; Takeda, S.; Hasegawa, T.; Nakamura, T.; Hosokoshi, Y.; Inoue, K.; Ikeuchi, S.; Miyazaki, Y.; Saito, K. *J. Am. Chem. Soc.* **2005**, *127*, 4397.
(7) (a) Nishihara, S.; Akutagawa, T.; Hasegawa, T.; Nakamura, T. *Chem. Commun.* **2002**, *5*, 408. (b) Akutagawa, T.; Hashimoto, A.; Nishihara, S.; Hasegawa, T.; Nakamura, T. J. *Supramol. Chem.* **2002**, *2*, 175. (c) Akutagawa, T.; Hashimoto, A.; Nishihara, S.; Hasegawa, T.; Nakamura, T. *J. Phys. Chem. B.* **2003**, *107*, 66. (d) Akutagawa, T.; Matsuura, K.; Hashimoto, A.; Nakamura, T. *Inorg. Chem.* **2005**, *44*, 4454. (e) Nishihara, S.; Akutagawa, T.; Sato, D.; Takeda, S.; Noro, S.; Nakamura, T. *Chem. Asian J.* **2007**, *2*, 1983.
(8) (a) Sato, D.; Akutagawa, T.; Takeda, S.; Noro, S.; Nakamura, T. *Inorg. Chem.* **2007**, *46*, 363. (b) Akutagawa, T.; Sato, D.; Koshinaka, H.; Aonuma, M.; Noro, S.; Takeda, S.; Nakamura, T. *Inorg. Chem.* **2008**, *47*, 5951. (c) Akutagawa, T.; Koshinaka, H.; Sato, D.; Takeda, S.; Noro, S.; Takahasi, H.; Kumai, R.; Tokura, Y.; Nakamura, T. *Nat. Mater.* **2009**, *8*, 342. (d) Akutagawa, T.; Koshinaka, H.; Ye, Q.; Noro, S.; Kawamata, J.; Yamaki, H.; Nakamura, T. *Chem. Asian J.* **2010**, *5*, 520.
(9) (a) Dominguez, Z.; Dang, H.; Strouse, M. J.; Garcia-Garibay, M. A. *J. Am. Chem. Soc.* **2002**, *124*, 2398. (b) Dominguez, Z.; Khuong, T. V.; Dang, H.; Sanrame, C. N.; Nuñez, J. E.; Garcia-Garibay, M. A. *J. Am. Chem. Soc.* **2003**, *125*, 8827. (c) Karlen, S. D.; Ortiz, R.; Chapman, O. L.; Garcia-Garibay, M. A. *J. Am. Chem. Soc.* **2005**, *127*, 6554. (d) Garcia-Garibay, M. A. *Proc. Natl. Acad. Sci. U.S.A.* **2005**, *102*, 10771. (e) Khuong, T. V.; Nuñez, J. E.; Godinez, C. E.; Garcia-Garibay, M. A. *Acc. Chem. Res.* **2006**, *39*, 413.
(10) Corey, E. J.; Feiner, N. F. *J. Org. Chem.* **1980**, *45*, 757.

Scheme 2. Molecular Structures of (1*R*,2*R*)-Cyclohexanediammonium ($CHDA^{2+}$) Dication, [18]Crown-6, Benzo[18]crown-6 (B[18]crown-6), Dibenzo[18]crown-6 (DB[18]crown-6), Cyclohexano[18]crown-6 (DCH-[18]crown-6), and $[Ni(dmit)_2]^-$

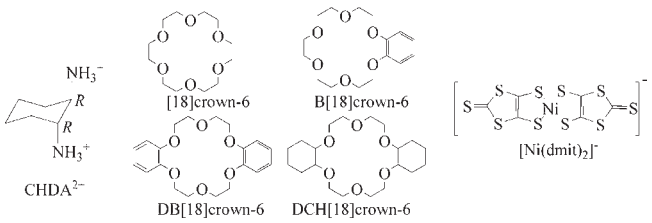

HBF_4 (2 mL) was slowly dropped into a solution of (1*R*,2*R*)-cyclohexanediamine (700 mg) in CH_3OH (20 mL) over a period of 20 min. The solvent was removed in vacuo, and then the white precipitates were recrystallized from $CHCl_3$ - hexane (1:1). Anal. Calcd for $C_6H_{16}N_2B_2F_8$: C, 24.87; H, 5.56; N, 9.67. Found: C, 24.65; H, 5.71; N, 9.72.

Preparation of Salts 1, 2, 3, and 4. The precursor monovalent (n-Bu_4N)[$Ni(dmit)_2$] salt was prepared according to the literature.[11] The single crystals of salts **1** and **3** were obtained by the density-gradient diffusion method in a vial cell (~30 mL). The green solution of (n-Bu_4N)[$Ni(dmit)_2$] (20 mg) in CH_3CN (15 mL) was layered on top of the mixed solution of ($CHDA^{2+}$)-(BF_4^-)$_2$ (40 mg) and crown ethers (~200 mg) in CH_3CN (15 mL). After four or five days, black blocks suitable for X-ray structural analyses were obtained. The single crystals of salts **2** and **4** were obtained by the standard diffusion methods using an *H*-shaped cell (50 mL). The green solution of (n-Bu_4N)-[$Ni(dmit)_2$] (20 mg) in CH_3CN (25 mL) and a solution of ($CHDA^{2+}$)(BF_4^-)$_2$ (40 mg) in the presence of crown ethers (~200 mg) in CH_3CN (25 mL) were slowly diffused at ambient conditions. After one week, black blocks suitable for X-ray structural analyses were obtained. Anal. Calcd for salt **1**, $C_{21.5}H_{32.5}O_6S_{10}N_{1.25}Ni$: C, 32.94; H, 4.18; N, 2.23. Found: C, 32.85; H, 3.96; N, 2.34. Anal. Calcd for salt **2**, $C_{26}H_{33.5}O_6S_{10}N_{1.5}Ni$: C, 37.07; H, 4.01; N, 2.49. Found: C, 37.12; H, 4.11; N, 2.33. Anal. Calcd for salt **3**, $C_{29}H_{32}O_6S_{10}N_1Ni$: C, 40.04; H, 3.71; N, 1.61. Found: C, 39.98; H, 3.76; N, 1.59. Anal. Calcd for salt **4**, $C_{29}H_{44}O_6S_{10}N_1Ni$: C, 39.49; H, 5.03; N, 1.59. Found: C, 39.30; H, 4.98; N, 1.64.

Crystal Structure Determination. Crystallographic data (Table 1) were collected by a Rigaku RAXIS-RAPID diffractometer using Mo−Kα (λ = 0.71073 Å) radiation from a graphite monochromator. Structure refinements were made using the full-matrix least-squares method on F^2. Calculations were performed using Crystal Structure software and SHELXL packages.[12] Parameters were refined using anisotropic temperature factors except for the hydrogen atoms.

Magnetic Susceptibility. The temperature-dependent magnetic susceptibility and the magnetization magnetic field dependence were measured using a Quantum Design MPMS-XL5 SQUID magnetometer using polycrystalline samples. The applied magnetic field was 1 T for all temperature-dependent measurements.

Calculations. The relative energies of ($CHDA^{2+}$)(crown ethers)$_2$ structures were calculated using the RHF/6-31(*d*) basis set (see Figure S7, Supporting Information).[13a] The atomic coordinates based on the X-ray crystal structural analysis were used for the calculations. The relative energy of the structures was obtained by evaluating the rigid pendulum motion of the $CHDA^{2+}$ cation around the nitrogen−nitrogen (N−N) direction. Pendulum motions were performed at every 5° along the forward−backward direction, and the relative energies were calculated using fixed atomic coordinates. The transfer integrals (t) between the $[Ni(dmit)_2]^-$ anions were calculated within the tight-binding approximation using the extended Hückel molecular orbital method. The LUMO of the $[Ni(dmit)_2]^-$ molecule was used as the basis function.[13b] Semiempirical parameters for Slater-type atomic orbitals were obtained from the literature.[13b] The t values between each pair of molecules were assumed to be proportional to the overlap integral (S) via the equation $t = -10S$ eV.

Dielectric Measurements. Temperature-dependent dielectric constants were measured by the two-probe AC impedance method at the frequencies of 1, 10, 100, and 1000 Hz (HP4194A). A single crystal was placed into a cryogenic refrigerating system (Daikin PS24SS). The electrical contacts were prepared using gold paste (Tokuriki 8560) to attach the 10-μm ϕ gold wires to the single crystal.

Results and Discussion

Four $[Ni(dmit)_2]^-$ salts of ($CHDA^{2+}$)([18]crown-6)$_2$-$[Ni(dmit)_2]_2^-(CH_3CN)_{0.5}$ (**1**), ($CHDA^{2+}$)(B[18]crown-6)$_2$-$[Ni(dmit)_2]_2^-(CH_3CN)$ (**2**), ($CHDA^{2+}$)(DB[18]crown-6)$_2$-$[Ni(dmit)_2]_2^-$ (**3**), and ($CHDA^{2+}$)(DCH[18]crown-6)$_2$-$[Ni(dmit)_2]_2^-$ (**4**) were obtained by cation exchange reactions. The monovalent state of $[Ni(dmit)_2]^-$ bearing one $S = 1/2$ spin in salts **1**−**4** was confirmed by the electronic absorption spectra (see Figure S2, Supporting Information). Reflecting the chiral structure of $CHDA^{2+}$, the crystals **1**−**4** had a chiral space group of $P1$. Although the $CHDA^{2+}$ and the $[Ni(dmit)_2]^-$ ions possessed common structural units in salts **1**−**4**, the changes in size and shape of the crown ethers modified the overall cation−anion packing structure.

Cationic Structures. Figure 1 summarizes the structures of sandwich-type ($CHDA^{2+}$)(crown ethers)$_2$ supramolecular cations in salts **1**−**4**. No disorder was observed in $CHDA^{2+}$ and crown ethers in salts **1**−**4** at 100 K. In all crystals, the cyclohexane ring adopted the (*a*,*a*)-conformation resulting in sandwich-type supramolecular cations. Table 2 summarizes selected structural parameters of the supramolecular cations. The dihedral angles of the N−C−C−N bond of $CHDA^{2+}$ in salts **1**−**4** (θ_{NCCN}, deg) were observed within the range of 160−163 deg. The $N-H^+-O$ hydrogen-bonding interactions between the ammonium moieties of $CHDA^{2+}$ and the six oxygen atoms of the crown ethers effectively formed supramolecular cations. The average N−O distance (d_{N-O}, degree) in salts **1**−**4** were within the range from 2.92 to 3.03 Å, suggesting standard hydrogen bonds in the formation of the supramolecules.[14] The steric hindrance between the cyclohexane ring and the two upper and lower crown ethers deformed the overall cationic structures, whereas the two crown

(11) Steimecke, G.; Sieler, H. J.; Krimse, R.; Hoyer, E. *Phosphorus Sulfur* **1979**, *7*, 49.

(12) (a) *Crystal Structure: Single crystal structure analysis software*, Ver. 3.6; Rigaku Corporation and Molecular Structure Corporation: The Woodlands, TX, 2004. (b) Sheldrick, G. M. *SHELX97 Programs for Crystal Structure Analysis*; Universitat Göttingen: Göttingen, Germany, 1998.

(13) (a) Frisch, M. J. et al. *GAUSSIAN R03W*; Gaussian, Inc.: Pittsburgh, PA, 2003. (b) Mori, T.; Kobayashi, A.; Sasaki, Y.; Kobayashi, H.; Saito, G.; Inokuchi, H. *Bull. Chem. Soc. Jpn.* **1984**, *57*, 627.

(14) (a) Jeffrey, G. A. *An Introduction to Hydrogen Bonding*; Truhlar, D. G.; Ed.; Oxford University Press: New York, 1997. (b) Pimentel, G. C.; McClellan, A. L. *The Hydrogen Bond*; Freemann: San Francisco, 1960. (c) Hamilton, W. C.; Ibers, J. A. *Hydrogen Bonding in Solids*; Breslow, R.; Karplus, M., Eds.; Benjamin Inc: New York, 1968.

(15) Scott, J. C. *Semiconductor and Semimetals. Highly Conducting Quasi-One-Dimensional Organic Crystals*; Conwell, E., Ed.; Academic Press: New York, 1988; p 385.

Table 1. Crystal Data, Data Collection, and Reduction Parameters of Salts **1**−**4** at 100 K

	1	**2**	**3**	**4**
chemical formula	$C_{43}H_{65}N_{2.5}O_{12}S_{20}Ni_2$	$C_{52}H_{67}O_{12}N_3S_{20}Ni_2$	$C_{58}H_{64}O_{12}N_2S_{20}Ni_2$	$C_{58}H_{88}O_{12}N_2S_{20}Ni_2$
M.W.	1566.6	1684.7	1739.8	1763.9
space group	*P*1(#1)	*P*1(#1)	*P*1(#1)	*P*1(#1)
a, Å	13.6381(3)	11.8981(5)	13.4825(7)	13.8573(8)
b, Å	13.9684(3)	12.7022(7)	15.6703(10)	14.2894(7)
c, Å	38.4431(7)	23.6880(10)	19.4822(11)	22.5510(11)
α, deg	82.3647(7)	97.926(2)	86.7592(17)	102.2521(14)
β, deg	82.1529(9)	91.6030(10)	72.4103(14)	92.9166(17)
γ, deg	63.9837(8)	95.911(2)	67.9133(15)	114.7420(18)
V, Å^3	6497.8(2)	3523.7(3)	3628.1(4)	3913.7(4)
Z	4	2	2	2
D_{calc}, g·cm^{-1}	1.601	1.588	1.592	1.497
T(K)	100	100	100	100
μ, cm^{-1}	12.774	11.843	11.528	10.695
reflections measured	64705	54575	54423	60666
independent reflections	48689	27521	28189	30966
reflections used	48689	27521	29549	30966
Flack parameter	0.019(6)	0.013(18)	0.90(2)	−0.001(11)
R_{int}	0.033	0.069	0.091	0.039
R_1[a]	0.0408	0.0732	0.0909	0.0512
wR_2 (F^2)[a]	0.1273	0.2418	0.2948	0.1882
GOF	0.884	0.991	0.997	1.154

[a] $R = \sum||F_o| - |F_c||/\sum|F_o|$ and $Rw = \{\sum[w(|F_o|^2 - |F_c|^2)^2]/\sum w(F_o^2)^2\}^{1/2}$.

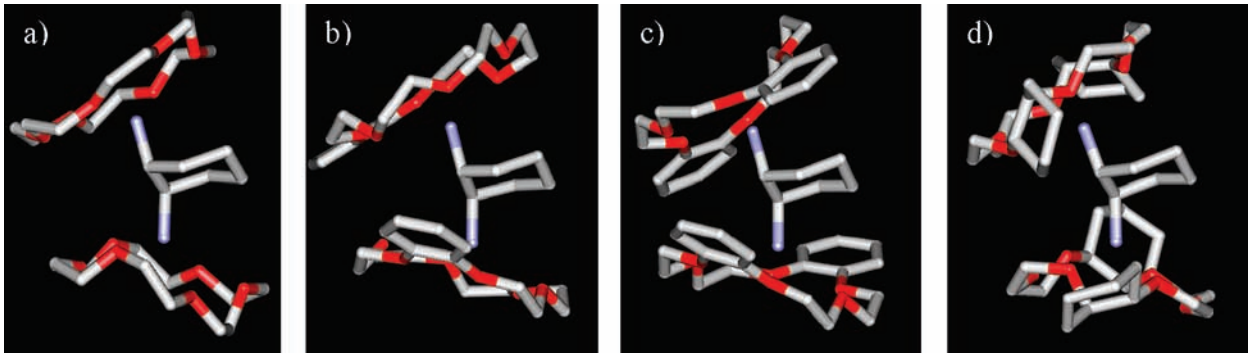

Figure 1. Supramolecular cationic structures of (a) ($CHDA^{2+}$)([18]crown-6)$_2$ in salt **1**, (b) ($CHDA^{2+}$)(B[18]crown-6)$_2$ in salt **2**, (c) ($CHDA^{2+}$)-(DB[18]crown-6)$_2$ in salt **3**, and (d) ($CHDA^{2+}$)(DCH[18]crown-6)$_2$ in salt **4**.

Table 2. Selected Structural Parameters of Supramolecular Cations of ($CHDA^{2+}$)-(crown ethers) in Salts **1**−**4** at 100 K

	1	**2**	**3**	**4**
d_{N-O}, Å[a]	2.96	2.95	2.92	3.02
θ_{crown}, deg[a]	46.7	45.9	46.5	47.1
θ_{NCCN}, deg[a]	160	163	163	161
V_c, Å^3[b]	611.6	681.5	753.4	808.6
V_c/V, %[b]	37.6	38.7	40.4	41.3

[a] The d_{N-O}, θ_{crown}, and θ_{NCCN} are the average N−O distance between $CHDA^{2+}$ and crown ethers, average angle between the two mean oxygen planes of crown ethers, and dihedral angle of the N−C−C−N bond of $CHDA^{2+}$ cation, respectively. [b] The volume V_c is the van der Waals volume of ($CHDA^{2+}$)(crown ethers)$_2$ supramolecules. The V_c/V was obtained by the ($V_c \times Z$)/unit cell volume (V). Here the Z is the number of cations within the unit cell.

ethers yielded open-mouth-shaped sandwich structures. The angles between the mean oxygen planes of the two crown ethers (θ_{crown}, deg) in salts **1**−**4** ranged from 45 to 48 deg. The van der Waals volume of ($CHDA^{2+}$)(crown ethers)$_2$ structures based on the crystal structures (V_c, Å^3) increased from 612, 682, and 753, to 809 Å^3 by changing the crown ethers from [18]crown-6, B[18]crown-6, and DB-[18]crown-6, to DCH[18]crown-6. The volume fraction of supramolecular cations within the unit cell also increased in the order of salt **1** (37.6%), **2** (38.7%), **3** (40.4%), to **4** (41.3%). The overall volume of the supramolecules in salts **1**−**4** affected the cation−anion packing structures in the crystals.

A 2-fold flip-flop motion of the aryl rings along the C−N axis has been observed for (anilinium)([18]crown-6), (anilinium)(DB[18]crown-6), and (*m*-fluoroanilinium)-(DB[18]crown-6) supramolecular structures in $[Ni(dmit)_2]^-$ salts.[8] The double-minimum rotational potentials for the flip-flop motion were determined by intermolecular interactions between two neighboring $[Ni(dmit)_2]^-$ anions and the π-plane of the aryl ring.[7,8] In the ($CHDA^{2+}$)(crown ethers)$_2$ supramolecules in salts **1**−**4**, the open-mouth-shaped sandwich structure restricted the 360° rotation of $CHDA^{2+}$ along the N−N direction due to the large steric hindrance. However, thermally activated large-amplitude motions of $CHDA^{2+}$ along the N−N direction were possible, from which the dielectric responses of salts **1**−**4** originated (see the section on dielectric properties). Although no disorder of $CHDA^{2+}$ was observed in the X-ray crystal structures of salts **1**−**4** at 100 K, the relatively large thermal parameters were distinct at 300 K due to the thermal fluctuations of $CHDA^{2+}$ (see Figures S5 and S6, Supporting Information). To estimate the thermally activated motions of $CHDA^{2+}$

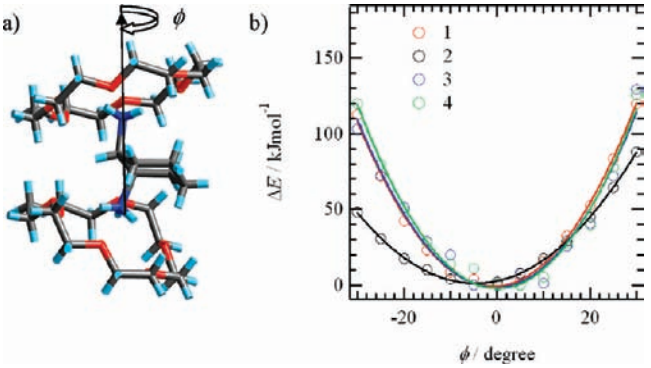

Figure 2. Potential energy curves for the cyclohexane ring pendulum motion along the N−N direction of the $CHDA^{2+}$ dication. (a) The calculated structure of $(CHDA^{2+})([18]crown-6)_2$ in salt **1**. The same $(CHDA^{2+})(crown\ ethers)_2$ units were evaluated for the salts **2**, **3**, and **4**. The movement axis was fixed along the N−N direction of the $CHDA^{2+}$ structure. (b) The $\Delta E - \phi$ dependences of salts **1** (red), **2** (black), **3** (blue), and **4** (green).

along the N−N direction, the potential energies were calculated using $(CHDA^{2+})(crown\ ethers)_2$ structures. The single point energy of the $(CHDA^{2+})(crown\ ethers)_2$ units were calculated by every 5-degree forward−backward pendulum motion from the atomic coordinates of X-ray crystal structural analyses at 100 K. Figure 2 shows the calculated structure of $(CHDA^{2+})(crown\ ethers)_2$ and the angle (ϕ) dependence of the potential energy (ΔE) of salts **1**−**4**.

The initial atomic coordinates obtained from the X-ray crystal structural analysis correspond to $\Delta E = 0$ kJ mol^{-1} and $\phi = 0°$. The single-minimum curve with relatively small curvature allows forward−backward pendulum motion of the cyclohexane ring of $CHDA^{2+}$. Almost symmetrical potential energy curves were observed in salts **1**, **3**, and **4**, whereas an asymmetrical profile was confirmed in salt **2** (black line in Figure 2b). In salt **2**, the $\Delta E = 90$ kJ mol^{-1} at $\phi = +30°$ was about twice as large as the $\Delta E = 50$ kJ mol^{-1} at $\phi = -30°$. The $\Delta E = 120$ kJ mol^{-1} for salts **1**, **3**, and **4** at $\phi = \pm 30°$ was the same as that for the rotational barrier of *m*-fluoroanilinium in the (*m*-fluoroanilinium)(dibenzo[18]crown-6)$[Ni(dmit)_2]^-$ salt,[8c] implying that forward−backward pendulum motion of $CHDA^{2+}$ within the range of $\phi_2 < \pm 30°$ was thermally induced around room temperature. The overall asymmetric potential $\Delta E - \phi$ profile of salt **2** indicates thermal motion of the $CHDA^{2+}$ dication.

Cation−Anion Packing Structures. Table 3 summarizes selected transfer integrals (t, eV) between the $[Ni(dmit)_2]^-$ anions, which were obtained by the extended Hückel molecular orbital calculation of the LUMO of $[Ni(dmit)_2]^-$. The magnitude of the absolute magnetic exchange energy ($|J|$) was estimated from the equation, $|J| \sim 4t^2/U_{eff}$, where U_{eff} is the effective on-site Coulomb repulsive energy of the $[Ni(dmit)_2]^-$ anions.[15]

Figure 3a shows the unit cell of salt **1**. Eight kinds of $[Ni(dmit)_2]^-$ anions (**A**, **B**, **C**, **D**, **E**, **F**, **G**, and **H**), four $CHDA^{2+}$ dications, and eight [18]crown-6 molecules comprised the crystallographically independent structural unit within the unit cell, resulting in a rather complicated molecular arrangement. The eight $[Ni(dmit)_2]^-$ ions were separated into three subunits of **A-B-C**, **D-E-F**, and **G-H**, which were arranged within the *ab*-plane through $\pi-\pi$, π−S, and lateral S−S interactions. Along the *c*-axis, several intermolecular interactions along the long axis of

Table 3. Selected Transfer Integrals (t, meV) of Salts **1**−**4** at 100 K[a]

	1	**2**	**3**	**4**
t_1	−9.29	18.3	143	104
t_2	−22.6	15.4	−25.1	−30.3
t_3	−5.21	5.62	37.8	7.32
t_4	−18.6	1.20	−8.39	8.00
t_5	−19.3	61.7	−8.40	−4.94
t_6	−0.18	2.65	−6.49	
t_7	12.9			

[a] The transfer integrals (t) were obtained by the LUMO of $[Ni(dmit)_2]^-$ based on the extended Hückel calculation ($t = -10S$ eV, where S is the overlap integral).

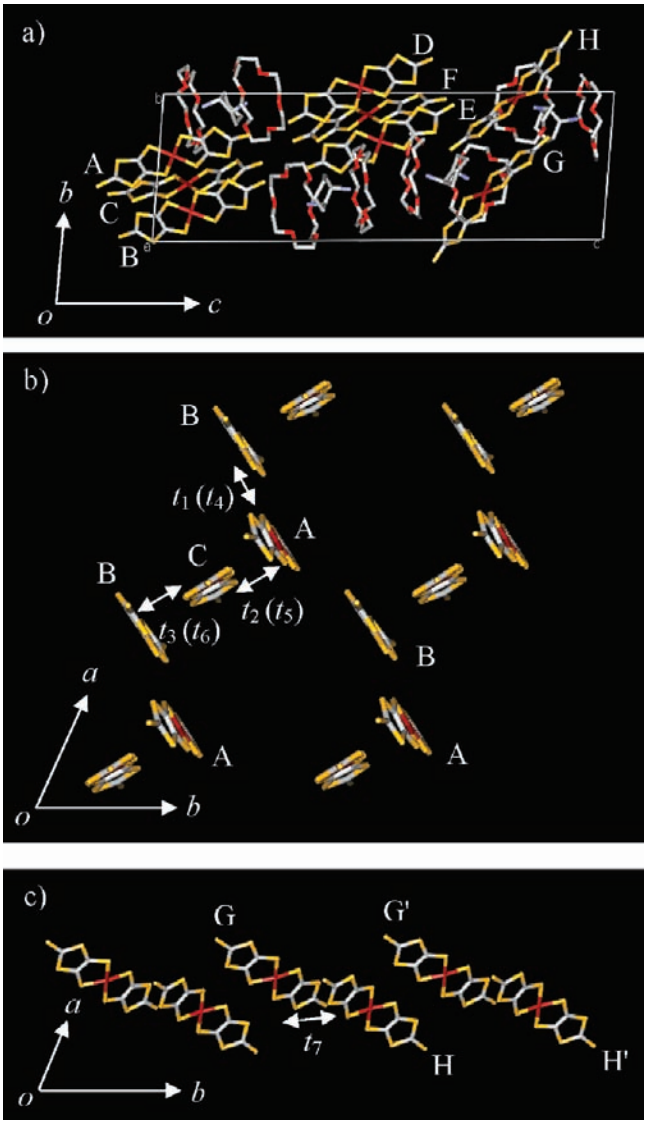

Figure 3. Crystal structure of salt **1**. (a) Unit cell viewed along the *a*-axis. The hydrogen atoms were omitted. Eight kinds of independent $[Ni(dmit)_2]^-$ anions existed in the unit cell. These were divided into three subunits of **A-B-C**, **D-E-F**, and **G-H**. (b) The $[Ni(dmit)_2]^-$ arrangements of the **A-B-C** subunit within the *ab*-plane. The **D-E-F** subunit also showed the same anion arrangement in the *ab*-plane. The $[Ni(dmit)_2]^-$ arrangements and transfer integrals ($t_4 - t_6$) in the **D-E-F** subunit layer are indicated in parentheses. (c) The $[Ni(dmit)_2]^-$ arrangements of the **G-H** subunit within the *ab*-plane.

the $[Ni(dmit)_2]^-$ were observed between the subunits. The molecular arrangements of the **A-B-C** and **D-E-F** subunits resembled each other (Figure 3b), where the **A-B** and **D-E**

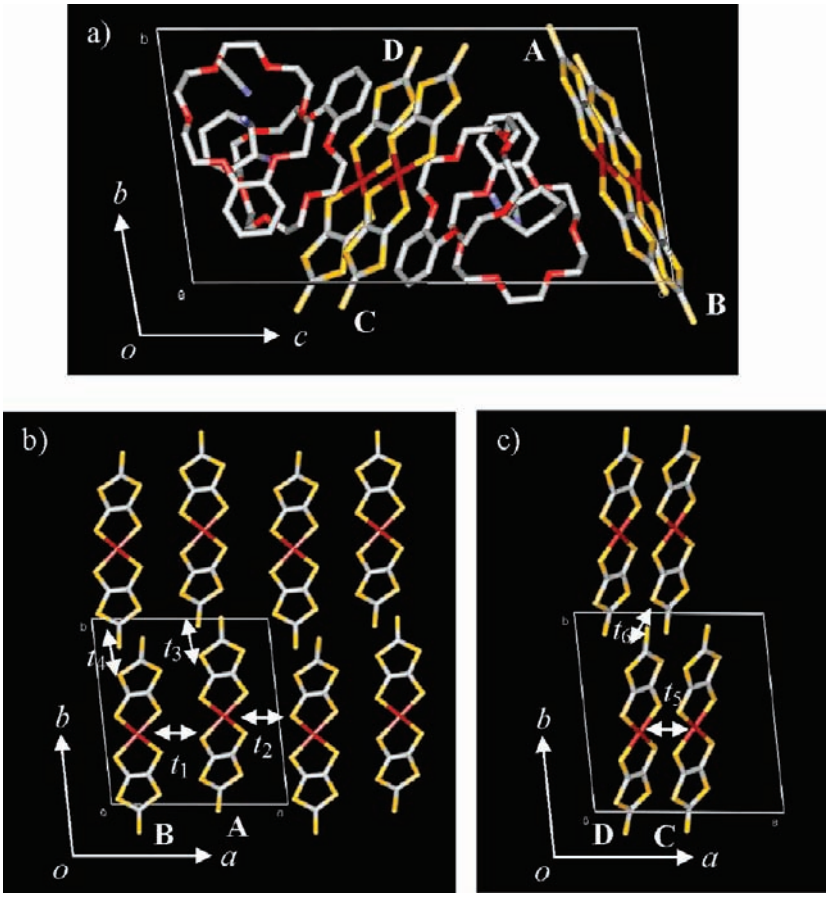

Figure 4. Crystal structure of salt **2**. (a) Unit cell viewed along the *a*-axis. The hydrogen atoms were omitted. Four independent $[Ni(dmit)_2]^-$ anions (**A**, **B**, **C**, and **D**) were divided into two subunits of **A-B** and **C-D**. (b) The $[Ni(dmit)_2]^-$ arrangements of the **A-B** subunit within the *ab*-plane viewed along the *c*-axis. (c) The $[Ni(dmit)_2]^-$ arrangements of the **C-D** subunit within the *ab*-plane viewed along the *c*-axis.

pairs formed lateral dimers along the short axis of the anion. The dimer interaction of **A-B** ($t_4 = -9.29$ meV) was half that of **D-E** ($t_1 = -18.6$ meV). The peripheral sulfur atoms of the **C** (**F**) interacted orthogonally with the π-plane of **A** and **B** (**D** and **E**). In the **A-B-C** subunit, the interaction of the **A-C** ($t_2 = -22.6$ meV) was larger than that of the **B-C** ($t_3 = -5.21$ meV) at 100 K. The **A-B-C** subunit corresponded to the **D-E-F** one, where the interaction of the **D-F** ($t_5 = -19.3$ meV) was much larger than that of the **E-F** ($t_6 = -0.16$ meV). Figure 3c shows the $[Ni(dmit)_2]^-$ (**G** and **H**) arrangements viewed along the *c*-axis. The intermolecular interactions ($t_7 = 12.9$ meV) between the **G** and **H** anions occurred at the terminal π-plane of the $[Ni(dmit)_2]^-$ anions. Each **G-H** subunit was isolated from the **A-B-C** and **E-F-G** subunits.

Figure 4 summarizes the crystal structure of salt **2**. The four kinds of crystallographically independent $[Ni(dmit)_2]^-$ anions (**A**, **B**, **C**, and **D**) were divided by two crystallographically independent $(CHDA^{2+})(B[18]crown\text{-}6)_2$ supramolecules into two subunits of **A-B** and **C-D** within the *ab*-plane. No effective intermolecular interactions between the **A-B** and **C-D** subunits were observed along the *c*-axis. Figure 4b,c shows the $[Ni(dmit)_2]^-$ arrangements of the **A-B** and **C-D** subunits within the *ab*-plane, showing different types of anion arrangements in the unit cell. The **A-B** subunit formed a chain through the lateral S−S interactions ($t_1 = 18.3$ and $t_2 = 15.4$ meV) along the *a*-axis. Along the *b*-axis, the weak intermolecular interactions of $t_3 = 5.62$ and $t_4 = 1.20$ meV connected each $[Ni(dmit)_2]^-$ along the long axis, resulting in a two-dimensional anion layer within the *ab*-plane. The **C-D** subunit formed strong π-dimers with $t_5 = 61.7$ meV (Figure 4c), which were connected through the S−S contact along the long axis ($t_6 = 2.69$ meV). The most effective intermolecular interaction in salt **2** was within the π-dimer of the **C-D** unit.

Four kinds of crystallographically independent $[Ni(dmit)_2]^-$ anions (**A**, **B**, **C**, and **D**) were observed in salt **3**. Figure 5a shows the unit cell of salt **3** viewed along the *b*-axis. The four **A-B-C-D** anions in salt **3** interacted with each other within the $(\bar{1}\,1\,1)$-plane, forming a two-dimensional layer. The $(CHDA^{2+})$(DB[18]crown-6) supramolecules were arranged between the anionic layers without effective cation−anion interactions. In the anion layer, the **A-B** pair and **C-D** pair formed dimers through $\pi-\pi$ and lateral S−S interactions, respectively. The intermolecular interaction within the π-dimer **A-B** was relatively strong ($t_1 = 143$ meV) compared to that of the lateral **C-D** dimer ($t_2 = -25.1$ meV). The π-dimer **A-B** interacted with the lateral **C-D** dimer ($t_3 = 37.8$ and $t_4 = -8.39$ meV) along the $-a + b + c$ axis to form a chain. The **C-D** dimer further interacted with the neighboring **C-D** dimers through $t_5 = -8.40$ meV and $t_6 = -6.49$ meV interactions, forming a ladder along the *b*-axis.

The cation−anion arrangements in salt **4** were similar to that of salt **2**. Figure 6a shows the unit cell of salt **4** viewed along the *a*-axis. Four kinds of crystallographically

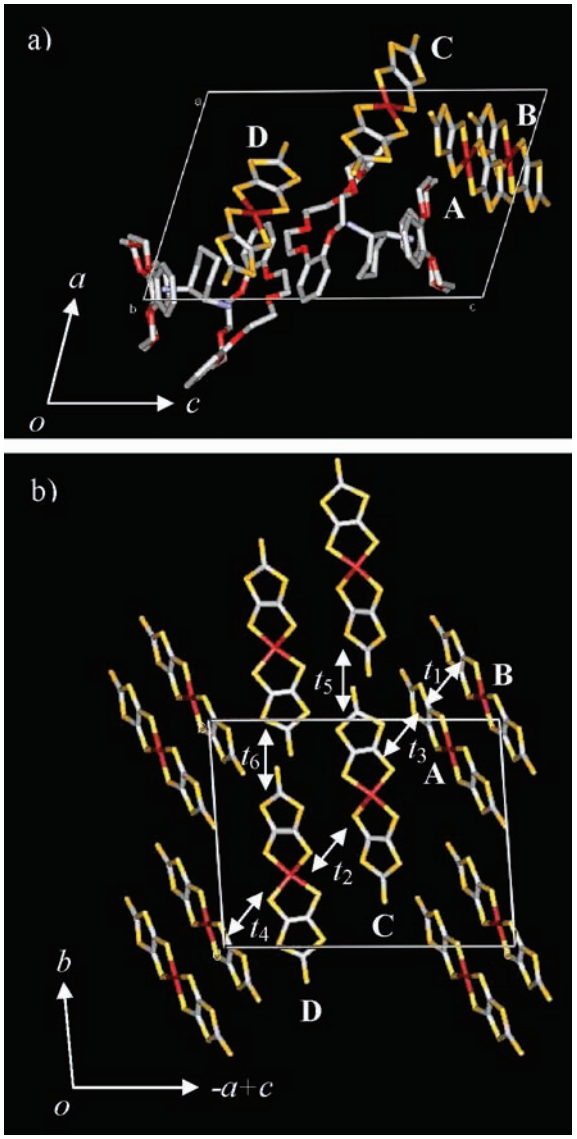

Figure 5. Crystal structure of salt **3**. (a) Unit cell viewed along the *b*-axis. The hydrogen atoms were omitted. Four independent $[Ni(dmit)_2]^-$ anions (**A**, **B**, **C**, and **D**) existed in the unit cell. (b) The $[Ni(dmit)_2]^-$ arrangements in the $(\bar{1}\ 1\ 1)$ plane, forming a two-dimensional anionic layer.

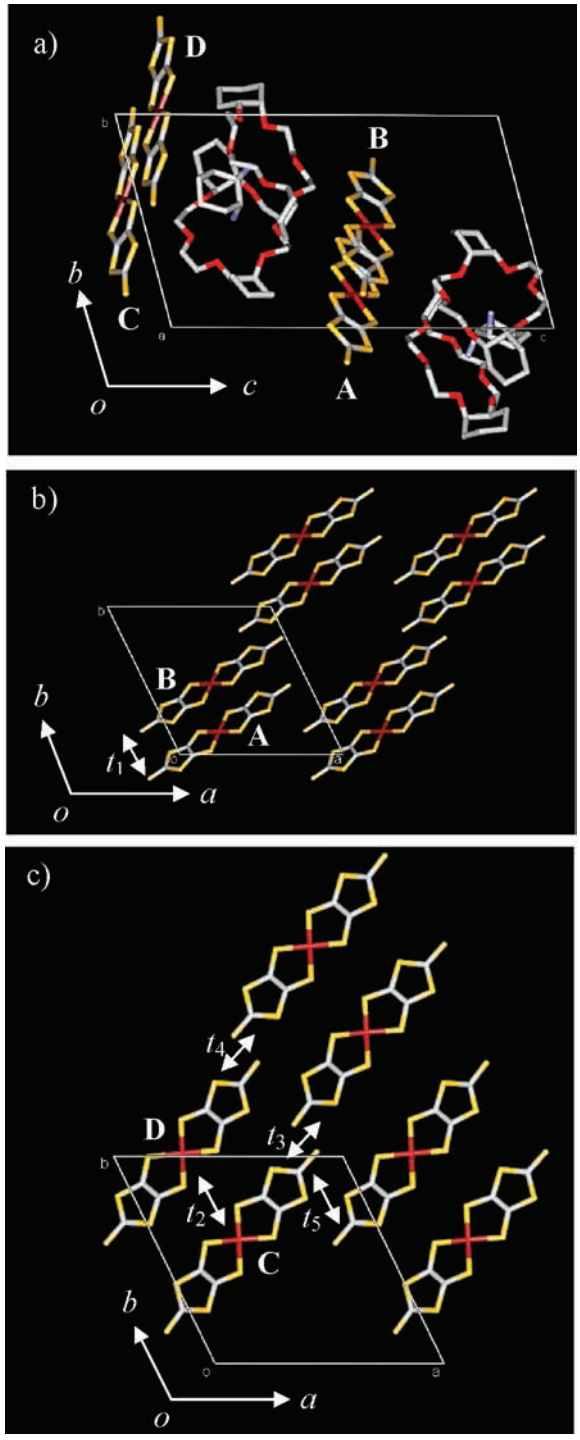

Figure 6. Crystal structure of salt **4**. (a) Unit cell viewed along the *a*-axis. The hydrogen atoms were omitted. Four independent $[Ni(dmit)_2]^-$ anions (**A**, **B**, **C**, and **D**) were divided into two subunits of **A-B** and **C-D**. (b) The $[Ni(dmit)_2]^-$ arrangements of the **A-B** subunit within the *ab*-plane viewed along the *c*-axis. (c) The $[Ni(dmit)_2]^-$ arrangements of the **C-D** subunit within the *ab*-plane viewed along the *c*-axis.

independent $[Ni(dmit)_2]^-$ anions (**A**, **B**, **C**, and **D**) were divided into two subunits of **A-B** and **C-D** within the *ab*-plane, forming independent two-dimensional anionic layers. The cation and anion layers were alternatively stacked along the *b*-*c* axis. The **A** and **B** anions formed a strong π-dimer with an intermolecular interaction of $t_1 = 104$ meV. Since an effective intermolecular interaction was not observed between the π-dimer, the **A-B** π-dimers were isolated from each other within the *ab*-plane. On the other hand, the **C** and **D** anions formed a lateral dimer ($t_2 = -30.3$ meV), which was further connected through the intermolecular interactions of $t_3 = 7.32$ and $t_4 = 8.00$ meV along the $a + b$ axis and $t_5 = -4.94$ along the *b*-axis. The lateral **C-D** dimer formed ladder-type molecular arrangements, where the ladder-leg and ladder-rung directions corresponded to the *b*- and $a + b$-axes, respectively. However, the intermolecular interaction along the ladder-leg was about 16 times larger than that along the ladder-rung direction, assuming the relation of $J \sim t^2$. Magnetic properties with such large anisotropies can be explained by the dimer model rather than the spin-ladder one (see the section on Magnetic Properties).

Magnetic Properties. Magnetic properties of salts **1**−**4** were determined by the $[Ni(dmit)_2]^-$ arrangements in the crystals. Table 4 summarizes the $[Ni(dmit)_2]^-$ arrangements and magnetic parameters of salts **1**−**4**. The magnetism of

Table 4. Magnetic Parameters of Salts **1**−**4**

	1	**2**	**3**	**4**
$[Ni(dmit)_2]^-$ arrangement	lateral dimer π−S interaction weak π-dimer	π-dimer lateral sheet	π-dimer ladder	π-dimer lateral sheet
g (298 K)[a]	2.0030	2.0048	2.0041	2.0085
ΔH (298 K), mT[a]	16.93	16.58	16.76	16.80
C, emu K mol^{-1}	0.376	0.340	0.391	0.352
θ or J/k_B, K	−8.2	−5.7	+3.1, −2.9	+2.8, −6.5
magnetism[b]	C−W	C−W	C−W + S−T	C−W + S−T

[a] g-value (g) and line width (ΔH) of the $[Ni(dmit)_2]^-$ anion were determined from the electron spin resonance spectra for single crystals at 298 K. [b] C−W and S−T are the Curie−Weiss and singlet−triplet thermal excitation models, respectively.

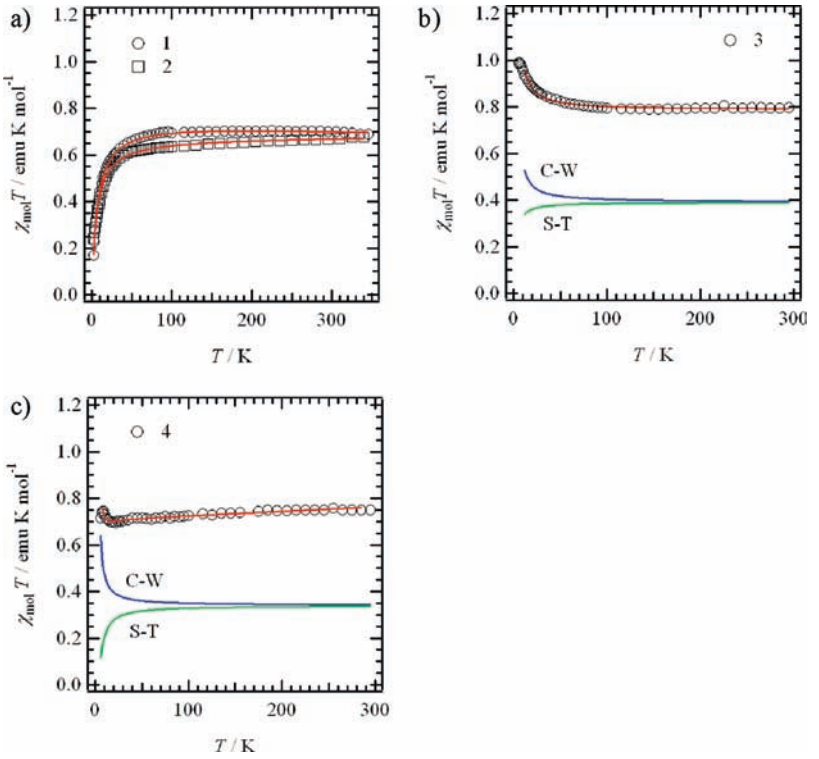

Figure 7. Temperature-dependent magnetic susceptibility of salts **1**−**4**. (a) The $\chi_{mol}T - T$ plots of salts **1** and **2**. The red lines were fit by the Curie−Weiss model. (b) The $\chi_{mol}T - T$ plots of salt **3**. The red line was divided into the two components of the Curie−Weiss model with ferromagnetic coupling (C−W: blue line) and the singlet - triplet thermal excitation model (S-T: green line). (c) The $\chi_{mol}T - T$ plots of salt **4**. The red line was fit by the sum of Curie−Weiss and singlet−triplet thermal excitation models (see text).

salts **1** and **2** obeyed the Curie−Weiss law with antiferromagnetic coupling (Figure 7a). The Weiss temperature (θ) of salts **1** and **2** were −8.2 and −5.7 K, respectively. Although different types of independent $[Ni(dmit)_2]^-$ layers were observed in salts **1** and **2**, the Curie−Weiss equation reproduced the χ_{mol} (molar magnetic susceptibility)$T - T$ behavior due to the weak intermolecular interactions. The $S = 1/2$ spin on $[Ni(dmit)_2]^-$ behaved almost independently in the salts.

Salts **3** and **4** showed an increase in $\chi_{mol}T$ upon decreasing temperature, suggesting a ferromagnetic interaction between the $[Ni(dmit)_2]^-$ anions. In salt **3**, rather strong π-dimers (**A-B**) and weakly interacting lateral dimers (**C-D**) were observed. Since the magnetism of the π-dimer **A-B** should follow the singlet−triplet (S−T) thermal excitation model,[16] the lateral **C-D** dimer should contribute to the ferromagnetic behavior of salt **3**. The $\chi_{mol}T - T$ plot of salt **3** was reproduced by the sum of the S−T dimer (green line in Figure 7b) and the Curie−Weiss model with the ferromagnetic coupling (blue line in Figure 7b). Assuming the same spin contribution from the **A-B** and **C-D** units, the magnetic exchange energy (J) of the **A-B** dimer (S−T model) and the Weiss temperature of the **C-D** dimer (Curie−Weiss model) were −12.9 and +3.1 K, respectively. The magnetic field (H) versus magnetization (M) curve at 2 K (Figure S8, Supporting Information) was consistent with the ferromagnetic coupling of two $S = 1/2$ spins.

In salt **4**, the π-dimer (**A-B**) and lateral dimer (**C-D**) should be magnetically independent from each other as indicated in the crystal structure. Magnetism of the π-dimer **A-B** should follow the singlet−triplet (S−T) thermal excitation model,[16] whereas the lateral **C-D** dimer may contribute to the ferromagnetic coupling. The $\chi_{mol}T - T$ plots of salt **4** were reproduced by the sum of the S−T dimer (green line in Figure 7c) and Curie−Weiss model with the ferromagnetic coupling (blue line in Figure 7c) as in the case of salt **3**. Assuming the same spin contribution from the **A-B** and **C-D** units, the magnetic

(16) (a) Carlin, R. L. *Magnetochemistry*; Springer-Verlag: Heidelberg, 1986. (b) Kahn, O. *Molecular Magnetism*; VCH: New York, 1993.

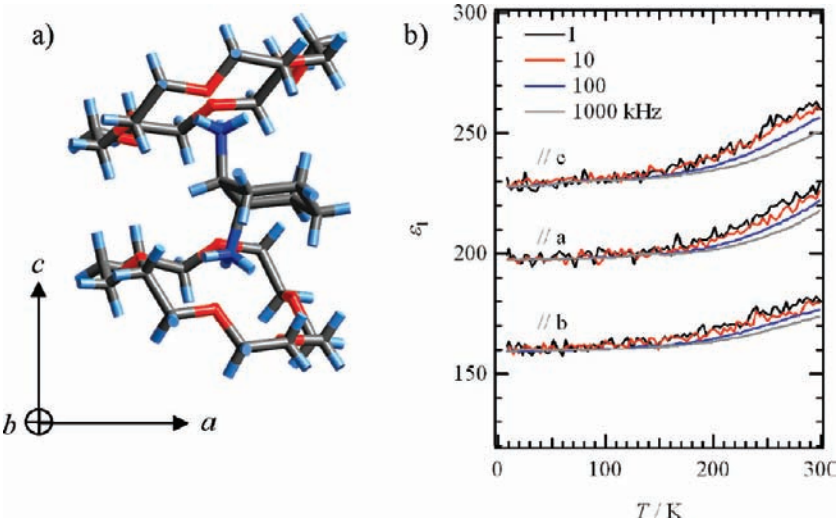

Figure 8. Dielectric properties of single crystal **1**. (a) The crystal *a*-, *b*-, and *c*-axes corresponded to the directions in the figure of $(CHDA^{2+})([18]crown\text{-}6)_2$ supramolecule. (b) Temperature- and frequency-dependent (f = 1, 10, 100, and 1000 kHz) dielectric constants (ε_1) along the *a*-, *b*-, and *c*-axes.

exchange energy (J) of the **A-B** dimer (S−T model) and the Weiss temperature of the **C-D** dimer (Curie−Weiss model) were −6.5 and +2.8 K, respectively.

Molecular Motion and Dielectric Properties. The temperature- and frequency-dependent dielectric constants (ε_1) of salts **1**−**4** were evaluated to confirm the molecular motion within the supramolecular cations.[17] When the frequency of the molecular motion in the crystal was on the order of the measurement frequency, large dielectric responses were expected. Since the structurally rigid $[Ni(dmit)_2]^-$ in salts **1**−**4** was insensitive to temperature and frequency in its dielectric responses, the flexible $(CHDA^{2+})(crown\ ether)_2$ structures must be responsible for the temperature and frequency dependence. The forward−backward motion of $CHDA^{2+}$ in the single-minimum-type potential energy was expected in the open-mouth-shaped $(CHDA^{2+})(crown\ ether)_2$ supramolecule (Figure 2). The potential energy of $CHDA^{2+}$ pendulum motion in salt **2** was lower than those of salts **1**, **3**, and **4**, suggesting a pendulum motion of $CHDA^{2+}$ at lower temperatures.

No distinct temperature and frequency dependences in dielectric responses of the single crystal were observed in salt **1** along the *a*-, *b*-, and *c*-axes (Figure 8). When the thermal pendulum motion of the cyclohexane ring occurred along the N−N direction of $CHDA^{2+}$, the dielectric responses along the *a*- and/or *b*-axis should be enhanced. However, only slight ε_1 enhancements were detected by increasing the temperature from the constant ε_1 values below 150 K: ε_1 (//*a*) = 200, ε_1 (//*b*) = 160, and ε_1 (//*c*) = 230. The anisotropy in the ε_1 values was related to the anisotropy of the π-electron distribution on $[Ni(dmit)_2]^-$, where the ε_1 value along the long axis of $[Ni(dmit)_2]^-$ was larger than those along the other directions due to larger polarization of the π-electron along the long axis. In salt **1**, the ε_1 value along the *c*-axis, along the long axis of $[Ni(dmit)_2]^-$, was larger than those along the *a*- and *b*-axes. Similar frequency-independent dielectric behaviors were observed in salts **3** and **4** (Figures S10 and S11, Supporting Information), where a slight ε_1 enhancement with no distinct frequency dependence appeared above 150 K. Salt **3** showed isotropic behavior with the ε_1 values (T < 150 K), which was in good accordance with the crystal structure with the $[Ni(dmit)_2]^-$ layer extended along the $(\bar{1}\ 1\ 1)$ plane (Figure 5). The long axis of each anion was distributed isotropically within the unit cell. The anisotropic behavior of ε_1 (//*a*) ~250, ε_1 (//*b*) ~230, and ε_1 (//*c*) ~120 of salt **4** at temperatures below 150 K was also consistent with the $[Ni(dmit)_2]^-$ arrangement with the long axis along the $a + b$ axis.

On the other hand, frequency-dependent behavior was observed in salt **2** along the *c*-axis. The asymmetrical single-minimum potential curve of salt **2** was different from those of salts **1**, **3**, and **4**. Figure 9a shows the correspondence between the $(CHDA^{2+})$(B[18]crown-6) orientation and crystal axes in the unit cell. The largest frequency- and temperature-dependent ε_1 behavior was observed along the *c*-axis (Figure 9b). Since the long axis of $[Ni(dmit)_2]^-$ was almost parallel to the *a*-axis, and the ε_1 along the *a*-axis was larger than that along the *c*-axis, the *c*-axis corresponded to the direction parallel to the cyclohexane ring and orthogonal to the pendulum motion axis. Figure 9c shows the $(CHDA^{2+})(B[18]crown\text{-}6)_2$ structure at the pendulum motion angles of ϕ = −30, 0, and +30°, respectively, used for the potential calculations. Larger steric hindrance between the cyclohexane ring and B[18]crown-6 at the ϕ = +30° (right in Figure 9c) than that at ϕ = −30° (left in Figure 9c) resulted in the asymmetrical $\Delta E - \phi$ profile in salt **2**. The large response in the low frequency measurement (f = 1 kHz) implies low frequency thermally induced molecular motion at higher temperatures, which is consistent with the lower potential energy of $CHDA^{2+}$ compared to the other three salts. Since the pendulum motion of the $CHDA^{2+}$ dication is not accompanied by a large change in the dipole moment, as in the cases of $(m\text{-fluoroanilinium})(DB[18]crown\text{-}6)[Ni(dmit)_2]^-$ and $(o\text{-aminoanilinium})(DB[18]crown\text{-}6)[Ni(dmit)_2]^-$ salts,[8c,d] the ε_1 enhancement at higher temperatures was relatively small.

(17) (a) *The Plastically Crystalline State*; Sherwood, J. N., Ed.; John Wiley & Sons: Chichester, 1979. (b) Hamilton, W. C.; Ibers, J. A. *Hydrogen Bonding in Solid*; W. A. Benjamin Inc.: New York, 1968. (c) Kao, K. C. *Dielectric Phenomena in Solids*; Elsevier: Amsterdam, 2004.

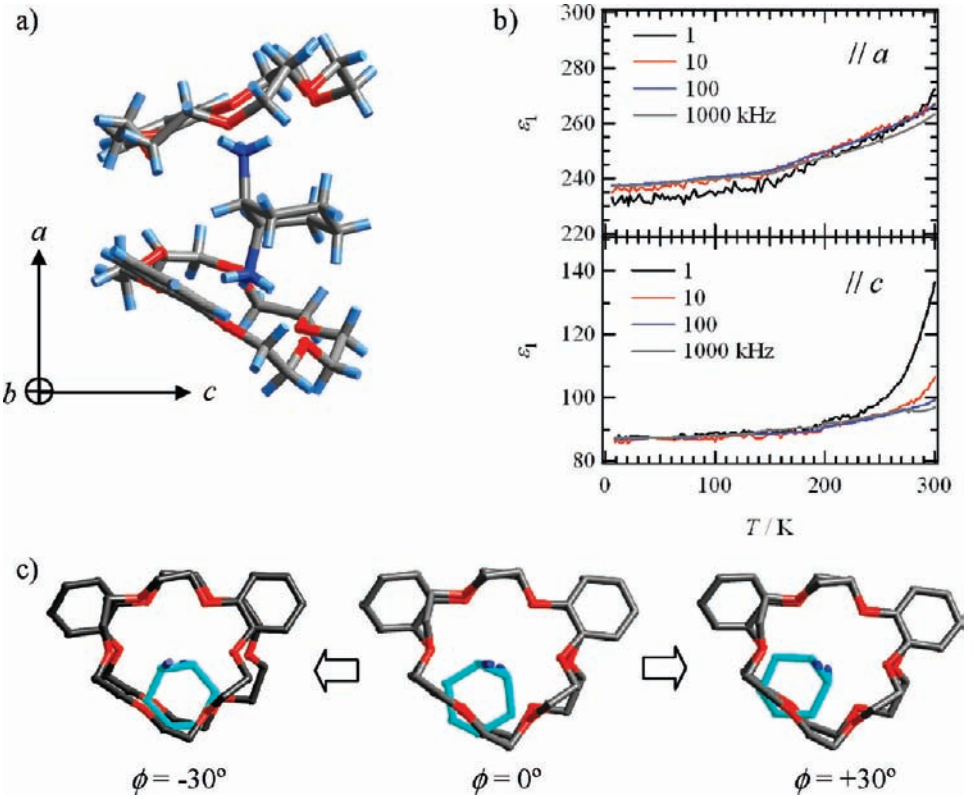

Figure 9. Dielectric properties of salt **2**. (a) The correspondence between the crystal *a*-, *b*-, and *c*-axes and $(CHDA^{2+})(B[18]crown\text{-}6)_2$ structure. (b) Temperature- and frequency-dependent (f = 1, 10, 100, and 1000 kHz) dielectric constants along the *a*- and *c*-axes. (c) The $CHDA^{2+}$ arrangements between the two upper and lower B[18]crown-6 molecules at the pendulum motion angles of the $\phi = -30, 0$, and $+30°$. The rigid movement of $CHDA^{2+}$ was assumed along the nitrogen−nitrogen direction of the dication.

Conclusions

Chiral (1*R*,2*R*)-cyclohexanediammonium ($CHDA^{2+}$) dication and four kinds of crown ethers of [18]crown-6, benzo[18]crown-6, dibenzo[18]crown-6, and dicyclohexano[18]crown-6 formed open-mouth-shaped supramolecular cations of $(CHDA^{2+})(crown\ ethers)_2$ through hydrogen bonding in $[Ni(dmit)_2]^-$ salts ($dmit^{2-}$ = 2-thioxo-1,3-dithiole-4,5-dithiolate). Complicated cation−anion arrangements were observed in the four salts of $(CHDA^{2+})([18]crown\text{-}6)_2[Ni(dmit)_2]^-_2(CH_3CN)_{0.5}$ (**1**), $(CHDA^{2+})(B[18]crown\text{-}6)_2[Ni(dmit)_2]_2^-(CH_3CN)$ (**2**), $(CHDA^{2+})(DB[18]crown\text{-}6)_2[Ni(dmit)_2]_2^-$ (**3**), and $(CHDA^{2+})(DCH[18]crown\text{-}6)_2[Ni(dmit)_2]_2^-$ (**4**). Thermally induced pendulum motion of the cyclohexane ring along the nitrogen−nitrogen (N−N) direction in the $(CHDA^{2+})(B[18]crown\text{-}6)_2$ structure occurred at higher temperatures, which was the origin of an enhancement of the dielectric response at low frequencies. The potential energy profile had a single-minimum with an asymmetrical shape, and this low curvature should be one of the sources of asymmetrical cationic motion at higher temperatures. Eight kinds of crystallographically independent $[Ni(dmit)_2]^-$ anions (**A**, **B**, **C**, **D**, **E**, **F**, **G**, and **H**) existed in the unit cell of salt **1**, whereas only four kinds of anions (**A**, **B**, **C**, and **D**) were independent structural units in salts **2**, **3**, and **4**. In salt **1**, the fundamental subunits of the **A-B-C**, **D-E-F**, and **G-H** formed independent anionic layers separated by the $(CHDA^{2+})([18]crown\text{-}6)_2$ supramolecules. Independent **A-B** and **C-D** anionic layers were observed in salts **2** and **4**, whereas intermolecular interactions in the **A-B-C-D** arrangement were observed in salt **3**. A variety of intermolecular $[Ni(dmit)_2]^-$ interactions such as π-dimer, lateral dimer along the short or long axis of anions, and ladder-arrangements coexisted in the crystals. These complicated $[Ni(dmit)_2]^-$ anion arrangements yielded complicated temperature-dependent magnetic behaviors. The magnetism of salts **3** and **4** were explained by the sum of the antiferromagnetically coupled **A-B** π-dimer and ferromagnetic coupling of the lateral **C-D** dimer. The asymmetrical chiral organic ammonium moiety of the flexible $CHDA^{2+}$ dication induced complicated $[Ni(dmit)_2]^-$ arrangements, which were essential to realize diverse magnetic responses that coexisted with dielectric responses in the molecular crystals.

Acknowledgment. This work was supported in part by a Grant-in-Aid for Science Research from the Ministry of Education, Culture, Sports, Science, and Technology of Japan and the National Natural Science Foundation of China (20701007). Y.Q. (JSPS P08040) thanks the Japan Society for the Promotion of Science.

Supporting Information Available: The atomic numbering scheme, structural analysis of salts **1**−**4**, IR spectra, and UV−vis-NIR spectra at room temperature are available free of charge via the Internet at http://pubs.acs.org.